Neurosci. Bull. July, 2020, 36(7):793–805
https://doi.org/10.1007/s12264-020-00502-w

www.neurosci.cn
www.springer.com/12264

ORIGINAL ARTICLE

Increased EZH2 Levels in Anterior Cingulate Cortex Microglia Aggravate Neuropathic Pain by Inhibiting Autophagy Following Brachial Plexus Avulsion in Rats

Xiang-Lei Meng[1,2,3] · Pengfei Fu[4] · Lin Wang[5] · Xun Yang[1,2,3] · Guanghui Hong[1,2,3] · Xin Zhao[1,2,3] · Jie Lao[1,2,3]

Received: 12 August 2019 / Accepted: 7 January 2020 / Published online: 28 April 2020

Abstract After brachial plexus avulsion (BPA), microglia induce inflammation, initiating and maintaining neuropathic pain. EZH2 (enhancer of zeste homolog 2) has been implicated in inflammation and neuropathic pain, but the mechanisms by which it regulates neuropathic pain remain unclear. Here, we found that EZH2 levels were markedly upregulated during BPA-induced neuropathic pain *in vivo* and *in vitro*, stimulating pro-inflammatory cytokines (IL-1β, TNF-α, and IL-6) secretion *in vivo*. In rats with BPA-induced neuropathic pain, mechanical and cold hypersensitivities were induced by EZH2 upregulation and inhibited by EZH2 downregulation in the anterior cingulate cortex. Microglial autophagy was also significantly inhibited, with EZH2 inhibition activating autophagy and reducing neuroinflammation *in vivo*. However, this effect was impaired by inhibiting autophagy with 3-methyladenine, suggesting that the MTOR signaling pathway is a functional target of EZH2. These data suggest that EZH2 regulates neuroinflammation and neuropathic pain *via* a novel MTOR-mediated autophagy signaling pathway, providing a promising approach for managing neuropathic pain.

Keywords EZH2 · Neuropathic pain · Autophagy · Brachial plexus avulsion · Neuroinflammation

Introduction

Neuropathic pain, defined as pain caused by a lesion or disease of the somatosensory system [1], reduces the quality of life and causes psychological diseases. Brachial plexus avulsion (BPA) is common in patients with high-energy trauma. Neuropathic pain is a common complication with a prevalence of 67%–71% in BPA patients [2]. The anterior cingulate cortex (ACC) is an important region of the brain [3] that has been found, in animal studies, to activate ACC–spinal dorsal horn projections, directly potentiate spinal sensory transmission, and generate neuropathic pain [4]. Yang *et al.* [5] reported that nerve injury-induced neuropathic pain elevates the intrinsic excitation of pyramidal neurons in the ACC of mice, suggesting that the ACC plays an important role in neuropathic pain. Microglia are the main type of immune cell in the central nervous system (CNS). Studies [6–8] have shown that microglia are activated to release pro-inflammatory cytokines, which are critical for initiating and maintaining neuropathic pain.

Enhancer of zeste homolog 2 (EZH2) is a crucial catalytic subunit of polycomb repressive complex 2 (PRC2), a methyltransferase that acts on histone H3 lysine27 (H3K27) to produce trimethylated H3K27 (H3K27TM), resulting in gene silencing. It has been suggested that EZH2 might be involved in the development

Electronic supplementary material The online version of this article (https://doi.org/10.1007/s12264-020-00502-w) contains supplementary material, which is available to authorized users.

✉ Jie Lao
laojiefd@sina.com

[1] Department of Hand Surgery, Huashan Hospital, Fudan University, Shanghai 200040, China

[2] Key Laboratory of Hand Reconstruction, Ministry of Health, Shanghai 200032, China

[3] Shanghai Key Laboratory of Peripheral Nerve and Microsurgery, Shanghai 200032, China

[4] Department of Neurosurgery, Huashan Hospital, Fudan University, Shanghai 200040, China

[5] Health Management Center, The First Affiliated Hospital of Zhengzhou University, Zhengzhou 450001, China

and maintenance of neuropathic pain by positively modulating pro-inflammatory cytokines *in vivo* [9]. Moreover, another study revealed that EZH2 might control inflammatory target genes by modulating the interferon regulatory factor (IRF) and signal transducer and activator of transcription (STAT) signaling pathways, which are well-established mechanisms that regulate inflammatory disorders *in vivo* and *in vitro* [10]. Recent evidence has suggested that microRNAs can negatively regulate neuroinflammation and neuropathic pain by binding to the 3′-untranslated region sequence of EZH2 [11]. Collectively, these studies indicate that EZH2-mediated signaling pathways are involved in the pathophysiology of neuropathic pain, and may help identify promising therapeutic strategies for treating neuropathic pain.

Autophagy is a crucial aspect of human health that has been shown to affect physiology, homeostasis, development, and lifespan [12]. It is an evolutionarily-conserved cellular process that delivers damaged organelles and long-lived proteins to the lysosome for degradation [13]. Evidence indicates that autophagy is involved in the modulation of neuropathic pain. One study reported that autophagy in GABAergic interneurons affects neuropathic pain [14], while another indicated that autophagy regulates neuropathic pain *via* the rapamycin-mediated mammalian target of rapamycin (MTOR) signaling pathway [15]. Moreover, microRNA has also been shown to contribute to neuropathic pain by modulating neuroinflammation *via* a novel mechanism in which it targets the *ATG14* gene [6]. Based on the findings of these studies, we hypothesized that autophagy plays an important role in the initiation and maintenance of neuropathic pain.

Although EZH2, autophagy, microglia, neuroinflammation, and the ACC may all be involved in neuropathic pain, the underlying molecular mechanisms remain elusive. In this study, we used the rat model of BPA-induced neuropathic pain to examine EZH2 expression, autophagy, and neuroinflammation in the ACC and to investigate the mechanism underlying neuropathic pain.

Materials and Methods

Animals and Neuropathic Pain Model

Adult male Sprague–Dawley rats weighing 200 ± 10 g were purchased from the Shanghai Laboratory Animal Research Center (Shanghai, China) and 3–4 rats per cage were maintained under specific pathogen-free conditions (23–24 °C, 12/12-h light/dark cycle, 40%–60% relative humidity). The rats were provided with food and water ad libitum and acclimated for one week prior to experiments. This study was approved by the Animal Ethics Committee of Fudan University, and all experimental procedures were carried out in accordance with the guidelines of the International Association for the Study of Pain. A total of 232 rats were used in this study and efforts were made to minimize the number of rats used.

Neuropathic pain was induced surgically in each rat following the procedure of Wang *et al.* [16]. Briefly, each rat was anesthetized with 1% sodium pentobarbital (40 mg/kg) and placed in a supine position with the head oriented close to the surgeon and the left forepaw abducted and extended. Using a scalpel, a 2-cm horizontal incision was made 2 mm above the clavicle, the superficial fascia was separated, and the sternocleidomastoid exposed. The sternocleidomastoid was then transected to expose the left brachial plexus, the C5-T1 spinal nerve roots were avulsed using mosquito forceps, and finally the incision was closed using 4-0 silk suture. The same procedure was performed on the sham-operated rats but the brachial plexus was left intact.

Isolation of ACC Microglia

Microglia were isolated from the ACC using the Percoll density gradient centrifugation method described by Willemen *et al.* [17]. Briefly, each rat was deeply anesthetized as above, then the ACC was dissected from the brain and transferred immediately into 4 mL of ice-cold Hanks' balanced salt solution. Next, the ACC suspension was passed through a 70-μm cell strainer (BD Biosciences, Alphen aan de Rijn, The Netherlands) and centrifuged at 400 × *g* for 7 min. The cells (4 mL) were then centrifuged in a density gradient consisting of 75% Percoll, 3 mL 50% Percoll, 3 mL 35% Percoll, and 2 mL PBS at 1000 × g and 10 °C for 20 min. Cells at the 50%/75% interface were collected, washed in ice-cold phosphate-buffered saline (PBS), and re-suspended in PBS containing 1% bovine serum albumin (BSA).

Pain Behavior Assessment

Measurement of Mechanical Allodynia

To assess mechanical allodynia, we measured the 50% mechanical withdrawal threshold (50% MWT) of the left hind paw according to the method described by Rubens *et al.* [18]. Briefly, each rat was placed on a metal mesh platform 30 cm above the floor and covered with a transparent plastic box. The rats were acclimatized for 30 min to reduce the effect of exploratory behavior on the measurements, which were carried out using Von Frey filaments (Stoelting, Wood Dale, IL) with bending forces of 0.4 g, 0.6 g, 1.0 g, 2.0 g, 4.0 g, 6.0 g, 8.0 g, and 15.0 g using Dixon's up-and-down method [19]. The 50% MWT

was assessed the day before surgery (day -1) and then on days 3, 7, and 14 post-surgery. Rats without evidence of pain after surgery were eliminated from the study.

Measurement of Cold Allodynia

To assess cold allodynia, we used the acetone spray test [20] with the same conditions and time points used to measure mechanical allodynia. Briefly, 250 μL of ice-cold acetone (0°C) was sprayed onto the center of the left hind paw. Then the cold withdrawal score (CWS) was determined according to the following criteria: 0, the paw did not respond to the cold acetone; 1, the paw responded mildly (withdrawal with little or no weight on paw); 2, the paw.

Intraperitoneal Drug Administration

GSK126, 3-methyladenine (3-MA), and rapamycin (Rapa) from APExBIO Technology (Houston, TX, USA) were dissolved in PBS with 5% dimethyl sulfoxide (DMSO). GSK126 (7 mg/kg), 3-MA (10 mg/kg), and Rapa (1 mg/kg) were intraperitoneally injected into the neuropathic pain or sham-operated rats once per day from day 1 to days 3, 7, or 14 after surgery.

Western Blot Analysis and Antibodies

To evaluate protein levels of EZH2, H3K27TM, p62, LC3 II (microtubule-associated protein 1A/1B-light chain 3), MTOR, phosphorylated MTOR (pMTOR), P70S6K, and phosphorylated P70S6K (pP70S6K), we carried out western blot analysis as described previously [9, 21]. Briefly, tissues or cells were collected and lysed with NP-40 lysis buffer (25 mmol/L Tris–HCl, 150 mmol/L NaCl, 1 mmol/L EDTA, 1% NP-40; pH 7.6) supplemented with a protease inhibitor cocktail, and protein concentration was quantified using BCA reagent. Protein samples (20 μg) were separated by sodium dodecyl sulfate–polyacrylamide gel electrophoresis, transferred onto nitrocellulose membranes, and incubated with primary antibodies (Table 1). Blots were developed with horseradish peroxidase-conjugated secondary antibodies and a chemiluminescent substrate on Kodak X-ray films (Rochester, NY, USA).

Quantitative Real-Time PCR (q-RT PCR)

Total RNA was extracted using TRIzol reagent (Invitrogen, Carlsbad, CA, USA) and reverse-transcribed using an M-MLV Reverse Transcriptase kit (Invitrogen, Carlsbad, CA, USA). Samples were then analyzed in triplicate by q-RT PCR using a standard SYBR Green PCR kit (Toyobo, Osaka, Japan) and a Rotor-Gene RG-3000A (Corbett Life Science, Sydney, New South Wales, Australia) according to each manufacturer's instructions. The primers used for q-RT PCR are listed in Table 2. Values were normalized to those of the housekeeping gene GAPDH and relative gene expression levels were quantified using the $2^{-\Delta\Delta Ct}$ method.

Enzyme-Linked Immunosorbent Assay (ELISA)

Protein samples were prepared for ELISA as for western blot analysis. The interleukin (IL)-1β, tumor necrosis factor (TNF)-α and IL-6 levels were determined using ELISA kits (R&D Systems, Minneapolis, MN, USA) according to the manufacturer's instructions.

Table 1 Information for primary antibodies

Name	Cat. number	Supplier	Application: dilution
Rabbit anti-EZH2	#5246	Cell Signaling Technology	WB: 1:1000 IF: 1:100
Mouse anti-NeuN	#94403	Cell Signaling Technology	IF: 1:100
Mouse anti-Iba-1	#MABN92	Millipore	IF: 1:100
Mouse anti-GFAP	#3670	Cell Signaling Technology	IF: 1:200
Rabbit anti-H3K27TM	#9733	Cell Signaling Technology	WB: 1:1000
Rabbit anti-p62	#39786	Cell Signaling Technology	WB: 1:1000 IF: 1:200
Rabbit anti-LC3	#3868	Cell Signaling Technology	WB: 1:1000
Rabbit anti-MTOR	#2983	Cell Signaling Technology	WB: 1:1000
Rabbit anti-pMTOR	#5536	Cell Signaling Technology	WB: 1:1000
Rabbit anti-P70S6K	#9202	Cell Signaling Technology	WB: 1:1000
Rabbit anti-pP70S6K	#9205	Cell Signaling Technology	WB: 1:1000
Mouse anti-β-actin	A5441	Sigma	WB: 1:5000

WB western blot, *IF* immunofluorescence

Table 2 Primers used for q-RT PCR

Gene	Forward (5′ → 3′)	Reverse (5′ → 3′)
GAPDH	CTGGGCTACACTGAGCACC	AAGTGGTCGTTGAGGGCAATG
EZH2	ACATCCTTTTCATGCAACACC	GTATCCACATCCTCAGCGGG
p62	AGCGTCAGGAAGGTGCCATT	CCTGTAGACGGGTCCACTTC

Immunofluorescence Analysis

To obtain tissue samples for immunofluorescence analysis, each rat was anesthetized and perfused through the ascending aorta with 200 mL heparinized PBS (0.01 mol/L, pH 7.35) followed by 4% paraformaldehyde. The brain was removed, fixed in 4% paraformaldehyde overnight, and dehydrated in 20% and 30% sucrose at 4 °C. Next, the brain was cut into 10-μm sections on a cryostat and those containing the ACC were collected. Immunofluorescence staining was performed according to the methods described by Yadav and Weng [9]. Briefly, the sections were blocked with 5% BSA containing 0.1% Triton X-100 for 1 h, incubated with primary rabbit polyclonal antibodies overnight at 4 °C, and then incubated with fluorescein isothiocyanate-conjugated secondary antibodies for 2 h at room temperature in the dark. The nuclei were stained and the sections mounted with Vectashield mounting medium [22]. Then the sections were examined using a fluorescence laser scanning confocal microscope (Leica, Wetzlar, Hessen, Germany).

Statistical Analysis

All data are presented as the mean ± SEM and GraphPad Prism 5.0 (GraphPad, San Diego, CA, USA) was used for statistical analysis. Between-group comparisons were performed using two-tailed unpaired *t*-tests with a 95% confidence interval set. Multiple comparisons were performed by one-way analysis of variance (ANOVA) followed by Tukey's or Dunnett's test to assess pairwise between-group differences. Behavioral data for each group were analyzed by repeated-measures ANOVA followed by Bonferroni's *post hoc* test. P values of < 0.05 were considered statistically significant.

Results

BPA Causes Mechanical and Cold Allodynia in Rats

Following BPA surgery, we performed behavioral assessments to establish that mechanical and cold allodynia had been induced in the rats before they were used for any biochemical assays. Rats with no observable neuropathic pain following BPA surgery were excluded from the study. Of the rats included in the study, the 50% MWT baseline (measured on the day before surgery) was 7.78 ± 0.26 g in the neuropathic pain (NeuP) group and 9.22 ± 1.34 g in the sham-operated (Sham) group, with no significant difference between them ($P > 0.05$). At all other time points studied (days 3, 7, and 14 post-surgery), the 50% MWT of the left hind paw in the NeuP group was significantly lower than their own baseline and the Sham group (Fig. S1A). The CWS baselines (measured the day before surgery) were 0.22 ± 0.11 in the NeuP group and 0.44 ± 0.11 in the Sham group ($P > 0.05$). At all other time points studied (days 3, 7, and 14 post-surgery), the CWS of the left hind paw in the NeuP group was significantly higher than their own baseline and the Sham group (Fig. S1B). Thus, these data showed that BPA causes neuropathic pain in rats.

EZH2 and H3K27TM Expression is Upregulated in Microglia *In Vivo* and *In Vitro*

Previously, Yadav and Weng [9] showed that spinal EZH2 expression is upregulated in rats with neuropathic pain following partial sciatic nerve ligation. They identified EZH2 as a crucial mediator of neuroinflammation and neuropathic pain treatment. However, it remains unclear whether EZH2 is upregulated in the ACC of rats with BPA-induced neuropathic pain. Here, we found that EZH2 was promptly upregulated in the ACC on day 3 post-surgery in the NeuP group and was sustained at higher levels than in the Sham group for 14 days (Fig. 1A). Consistent with these western blot findings, q-RT PCR analysis revealed that EZH2 mRNA expression was strongly induced on days 3, 7, and 14 post-surgery in the ACC of the NeuP group compared with the Sham group (Fig. 1B). To determine whether EZH2 overexpression enhanced its catalytic activity, we measured H3K27TM expression by western blot analysis. The ACC of rats in the NeuP group displayed higher H3K27TM expression on days 3, 7, and 14 post-surgery than the Sham group (Fig. 1C). Taken together, these data suggest that EZH2 activity is enhanced in the ACC of rats with BPA-induced neuropathic pain, but it remained unclear in which cell type EZH2 was expressed. To determine this, we examined the localization of EZH2 within the ACC sections from the NeuP group on day 3 post-surgery, and found that EZH2 overexpression was co-localized with Iba1 (ionized Ca^{2+}-binding adaptor

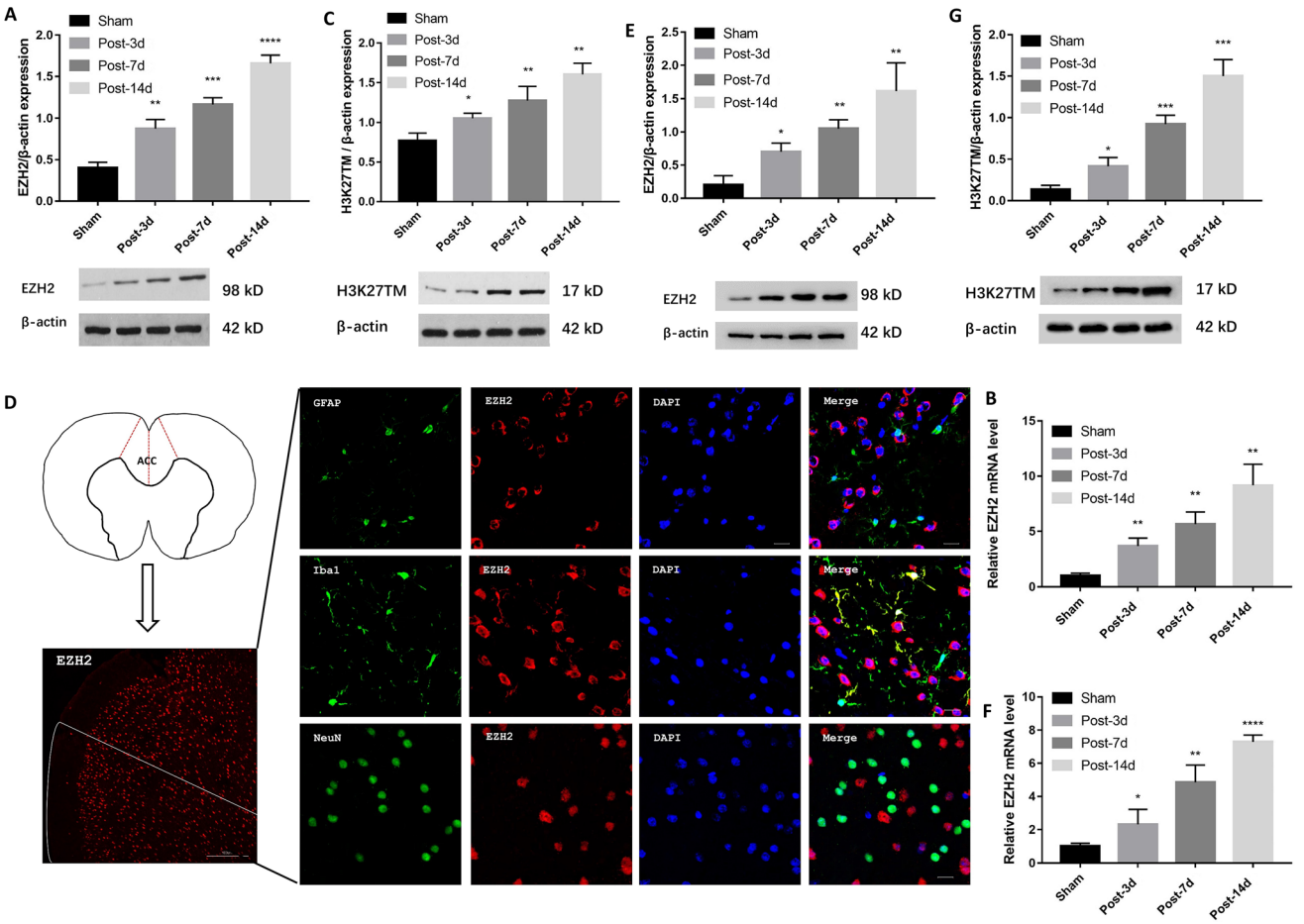

Fig. 1 Expression of EZH2 and H3K27TM is increased in microglia *in vivo* and *in vitro*. **A–C** The relative expression of EZH2 (**A**), EZH2 mRNA (**B**), and H3K27TM (**C**) in the ACC of the Sham and NeuP groups on days 3, 7, and 14 post-surgery (mean ± SD; $n = 8$; $^{*}P < 0.05$, $^{**}P < 0.01$, $^{***}P < 0.001$, $^{****}P < 0.0001$ *vs* Sham group). **D** Right panels, representative images of co-localization of EZH2 (red) with different cellular markers (green): GFAP for astrocytes, Iba1 for microglia, and NeuN for neurons (scale bar, 20 μm). Left panels, diagram of brain cross-section through the ACC, and low-magnification image of EZH2 in the ACC of the right hemisphere (scale bar, 100 μm). **E–G** Relative expression of EZH2 (**E**), EZH2 mRNA (**F**), and H3K27TM (**G**) in primary microglia from Sham and NeuP groups on days 3, 7, and 14 post-surgery (mean ± SD; $n = 3$; $^{*}P < 0.05$, $^{**}P < 0.01$, $^{***}P < 0.001$, $^{****}P < 0.0001$ *vs* Sham group).

molecule 1), a microglia-specific marker (Fig. 1D). To confirm that EZH2 was overexpressed in the ACC microglia, we isolated primary microglia from the ACC of Sham and NeuP rats on days 3, 7, and 14 post-surgery. We found that the EZH2 protein and mRNA levels and the H3K27TM levels were significantly upregulated in primary microglia from the ACC of the NeuP rats on each day post-surgery compared to those in the Sham rats (Fig. 1E–G).

Neuroinflammation is Increased in the ACC of Rats with BPA-Induced Neuropathic Pain

Microglia are the predominant type of immune cell in the CNS and express pro-inflammatory cytokines when activated by nerve injury. Therefore, we investigated the levels of pro-inflammatory cytokines secretion in the ACC of NeuP rats and found that the IL-1β, TNF-α, and IL-6 levels were markedly higher on days 3, 7, and 14 post-surgery than in Sham rats (Fig. 2A–C). These findings strongly suggest that increased neuroinflammation is positively correlated with EZH2 upregulation in the ACC of rats with BPA-induced neuropathic pain.

Autophagy is Suppressed in Microglia *In Vivo* and *In Vitro*

Previously, Shi *et al.* [6] showed that autophagy participates in neuropathic pain modulation and pro-inflammatory cytokines secretion. Here, we found that the expression of the autophagy-associated proteins LC3II and p62 changed in the ACC of NeuP rats on days 3, 7, and 14 post-surgery. Moreover, LC3II levels were markedly lower in the ACC

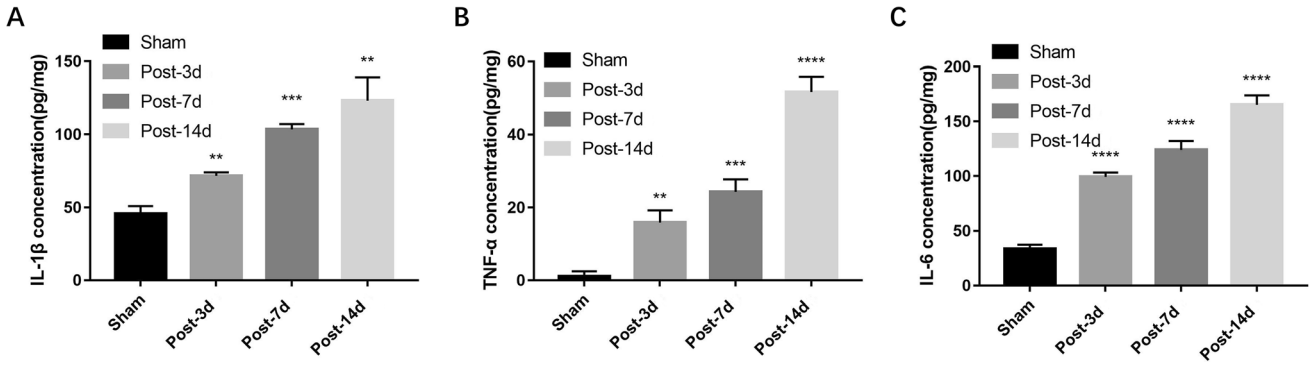

Fig. 2 Expression of pro-inflammatory cytokines is increased in the ACC of rats with BPA-induced neuropathic pain. **A–C** ELISA analysis showing the IL-1β (**A**), TNF-α (**B**), and IL-6 (**C**) expression levels in the ACC of Sham and NeuP rats on days 3, 7, and 14 post-surgery compared with Sham rats (mean ± SD; $n = 8$; $^{**}P < 0.01$, $^{***}P < 0.001$, $^{****}P < 0.0001$ *vs* Sham group).

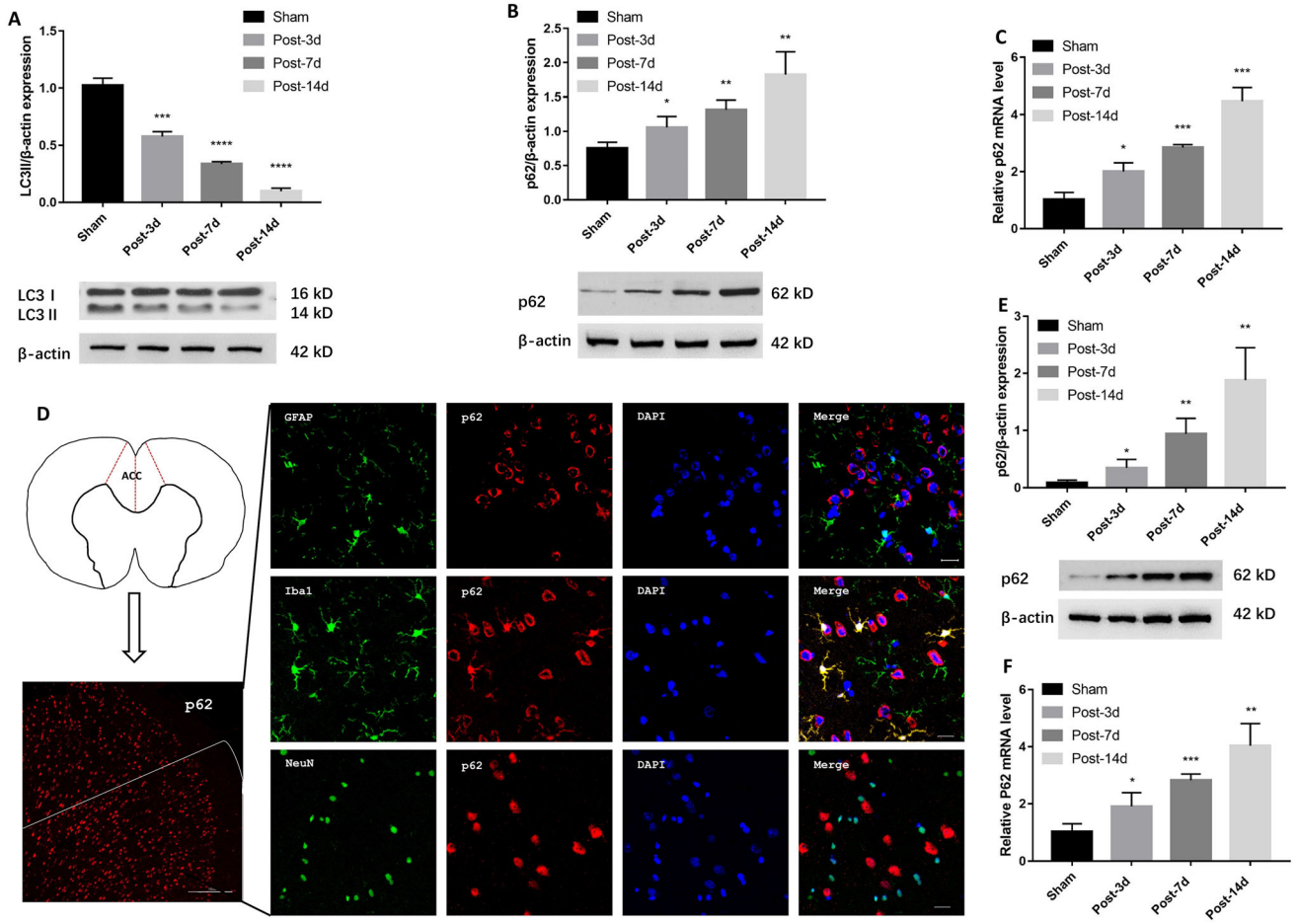

Fig. 3 Autophagy is inhibited in microglia *in vivo* and *in vitro*. **A–C** Relative expression of LC3II (**A**), p62 protein (**B**), and p62 mRNA (**C**) in the ACC of Sham and NeuP groups ($n = 8$ for each). **D** Right panels, representative images of co-localization of p62 (red) with different cellular markers (green): GFAP for astrocytes, Iba1 for microglia, and NeuN for neurons (scale bar, 20 μm). Left panels, diagram of brain cross-section with the ACC, and low-magnification image of p62 in the ACC of the left hemisphere (scale bar, 100 μm). **E, F** Relative expression of p62 (**E**) and p62 mRNA (**F**) in primary microglia ($n = 3$). Mean ± SD; $^{*}P < 0.05$, $^{**}P < 0.01$, $^{***}P < 0.001$, $^{****}P < 0.0001$ *vs* Sham group.

of NeuP rats on each of the days post-surgery than in Sham rats (Fig. 3A). Conversely, p62 levels progressively accumulated in the ACC of NeuP rats compared to Sham rats on each of the days post-surgery (Fig. 3B). Consistent with the western blot findings, p62 mRNA expression was strongly induced in the ACC of NeuP rats on each of the days post-

surgery (Fig. 3C), suggesting that the progress of autophagy is impaired in rats with BPA-induced neuropathic pain.

Consequently, we evaluated whether autophagy was impaired in the ACC microglia of NeuP rats. Fluorescence microscopic analysis of the ACC sections revealed that p62 accumulation was co-localized with Iba1, indicating that autophagy was mainly suppressed in the microglia (Fig. 3D). To confirm this finding, we isolated primary microglia from the ACC of NeuP and Sham rats on days 3, 7, and 14 after surgery. Consistent with the results from the ACC sections, the p62 protein and mRNA levels were significantly higher in the primary microglia from the NeuP rats on each of the days after surgery than those from the Sham rats (Fig. 3E, F). Taken together, these data suggest that autophagy is suppressed in the ACC microglia of rats with BPA-induced neuropathic pain.

EZH2 Inhibition Suppresses Neuroinflammation and Induces Autophagy

To further elucidate the function of EZH2 in the regulation of autophagy and whether inhibiting EZH2 has an analgesic effect, we examined autophagy activation after treating NeuP rats with GSK126, a selective EZH2 inhibitor. The inhibition of EZH2 by GSK126 attenuated the mechanical and cold allodynia in the NeuP rats compared to those without GSK126 treatment on days 3, 7, and 14 post-surgery (Fig. 4A, B). Meanwhile, GSK126 markedly inhibited the EZH2 and H3K27TM expression levels in the ACC of the Sham group compared with DMSO treatment on each of the days after surgery (Fig. 4C, D). Therefore, we investigated the relationship between EZH2, neuroinflammation, and autophagy activation. GSK126 downregulated the IL-1β, TNF-α, and IL-6 secretion levels in the ACC of NeuP rats on each of the days post-surgery compared to those treated with DMSO (Fig. 4E–G), whereas the LC3II levels were upregulated and p62 levels were downregulated in the ACC compared with DMSO treatment in the Sham group on each of the days post-surgery (Fig. 4H, I).

Autophagy Upregulation Suppresses Neuroinflammation and Neuropathic Pain

To better understand the exact role of autophagy activation in the ACC with respect to neuropathic pain, we treated NeuP rats with Rapa to validate the function of autophagy. Rapa reduced the mechanical and cold allodynia in these rats on days 3, 7, and 14 post-surgery (Fig. 5A, B) and upregulated LC3II expression in the ACC on each day compared to DMSO treatment (Fig. 5C). Consistent with this, the p62 protein levels were markedly downregulated in the ACC of NeuP rats following Rapa treatment on each of the days post-surgery (Fig. 5D). To further explore the relationship between autophagy and neuroinflammation, we measured the IL-1β, TNF-α and IL-6 secretion levels in the ACC of NeuP rats, and found that Rapa repressed neuroinflammation (Fig. 5E–G). Taken together, these data suggest that upregulation of autophagy can attenuate neuroinflammation and neuropathic pain.

EZH2 Negatively Regulates Autophagy in Rats with BPA-Induced Neuropathic Pain

To elucidate the relationship between EZH2 and autophagy, NeuP rats were intraperitoneally injected with both GSK126 and 3-MA once per day from day 1 to day 3 post-surgery. We found that the alleviation of mechanical (Fig. 6A) and cold allodynia (Fig. 6B) was reversed after treatment with both GSK126 and 3-MA compared with GSK126 treatment only, and there was no significant difference in the degree of mechanical and cold allodynia between the NeuP and 3-MA + GSK126 groups. These findings indicate that inhibiting autophagy with 3-MA impairs the pain relief induced by the EZH2 inhibitor. To determine the mechanism by which 3-MA impaired the pain relief induced by GSK126, we measured the EZH2 and H3K27TM expression levels using western blot analysis. EZH2 (Fig. 6C) and H3K27TM (Fig. 6D) expression was lower in the 3-MA + GSK126 group than in the NeuP group, but there was no significant difference between the 3-MA + GSK126 and GSK126 groups, indicating that 3-MA does not influence the GSK126-induced downregulation of EZH2 and H3K27TM. We also analyzed the expression of the autophagy-associated proteins LC3II and p62, and found that the LC3II levels (Fig. 6E) were downregulated in the 3-MA + GSK126 group compared to the GSK126 group and the p62 protein levels (Fig. 6F) were upregulated in the 3-MA + GSK126 group compared to the GSK126 group, indicating that 3-MA reversed the enhanced autophagy induced by GSK126. In addition, the IL-1β (Fig. 6G), TNF-α (Fig. 6H), and IL-6 (Fig. 6I) levels were higher in the 3-MA + GSK126 group than in the GSK126 group, but there was no significant difference between the 3-MA + GSK126 and NeuP groups, indicating that 3-MA also impaired the remission of inflammation induced by GSK126. In conclusion, these data indicate that inhibiting autophagy using 3-MA impairs EZH2-induced pain relief and neuroinflammation remission, suggesting that autophagy is a downstream target of EZH2, which aggravates neuroinflammation and neuropathic pain in rats with BPA-induced neuropathic pain.

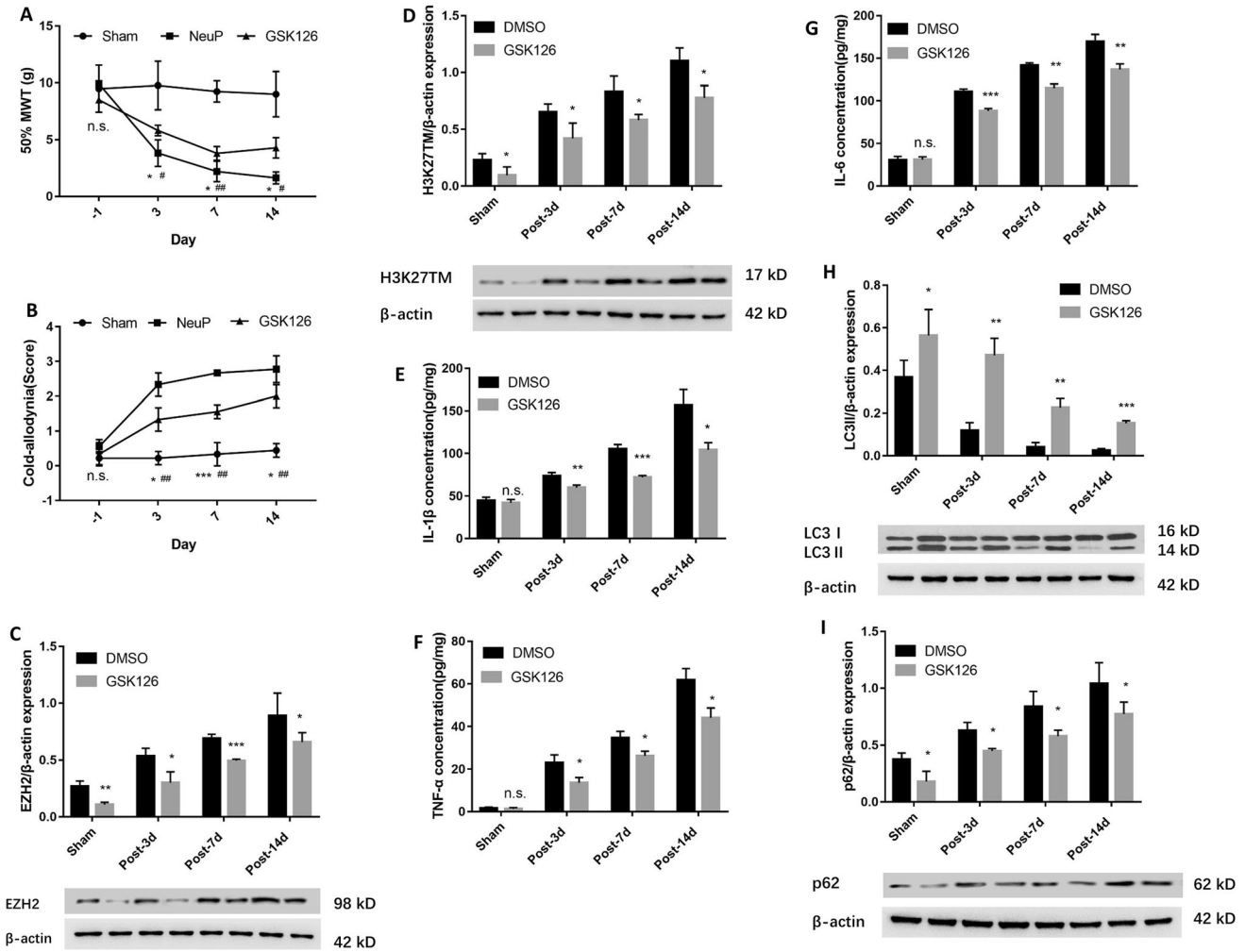

Fig. 4 Inhibition of EZH2 by GSK126 suppresses neuroinflammation and induces autophagy. **A**, **B** The 50%MWT (**A**) and CWS (**B**) in the Sham and NeuP groups after GSK126 treatment from day 3 to day 14 post-surgery (mean ± SD; $n = 8$; n.s., no significant difference among Sham, NeuP and GSK126 groups; $^{*}P < 0.05$, $^{**}P < 0.01$, $^{***}P < 0.001$ *vs* NeuP group; $^{\#}P < 0.05$, $^{\#\#}P < 0.01$ *vs* Sham group). **C**, **D** Relative expression of EZH2 (**C**) and H3K27TM (**D**) in the ACC of the Sham and NeuP groups after GSK126 treatment. **E**–**G** ELISA analysis of IL-1β (**E**), TNF-α (**F**), and IL-6 (**G**) expression levels in the ACC of the Sham and NeuP groups after GSK126 treatment from day 3 to day 14 post-surgery. **H**, **I** Relative expression of LC3II (**H**) and p62 protein (**I**) in the ACC of the Sham and NeuP groups after GSK126 treatment from day 3 to day 14 post-surgery. For **C**–**I**: mean ± SD; $n = 8$; n.s., no significant difference; $^{*}P < 0.05$, $^{**}P < 0.01$, $^{***}P < 0.001$ *vs* DMSO group.

EZH2 Regulates Autophagy *Via* an MTOR-Dependent Signaling Pathway

Previously, Wei *et al.* [21] showed that EZH2 epigenetically regulates autophagy in colorectal carcinoma cells *via* the MTOR signaling pathway, whose activation is known to suppress autophagy while its inhibition enhances autophagy. Therefore, we determined whether EZH2 upregulation inhibits autophagy *via* the MTOR pathway in the ACC microglia of rats with BPA-induced neuropathic pain. To do so, we measured pMTOR and pP70S6K expression levels, which are main markers of MTOR activity. The expression of both pMTOR and pP70S6K was upregulated in NeuP rats on days 3, 7, and 14 post-surgery compared with Sham rats (Fig. 7A, B). To confirm that EZH2 acts *via* the MTOR pathway, we intraperitoneally injected GSK126 into NeuP rats from day 1 to day 3 post-surgery, and found that MTOR activity was induced and the pMTOR and pP70S6K levels were reduced (Fig. 7C, D). These results indicate that EZH2 regulates autophagy *via* an MTOR-dependent signaling pathway.

Discussion

Neuropathic pain is unbearable and highly refractory, so treatments to attenuate it are important for improving the quality of life of patients following BPA. An increasing

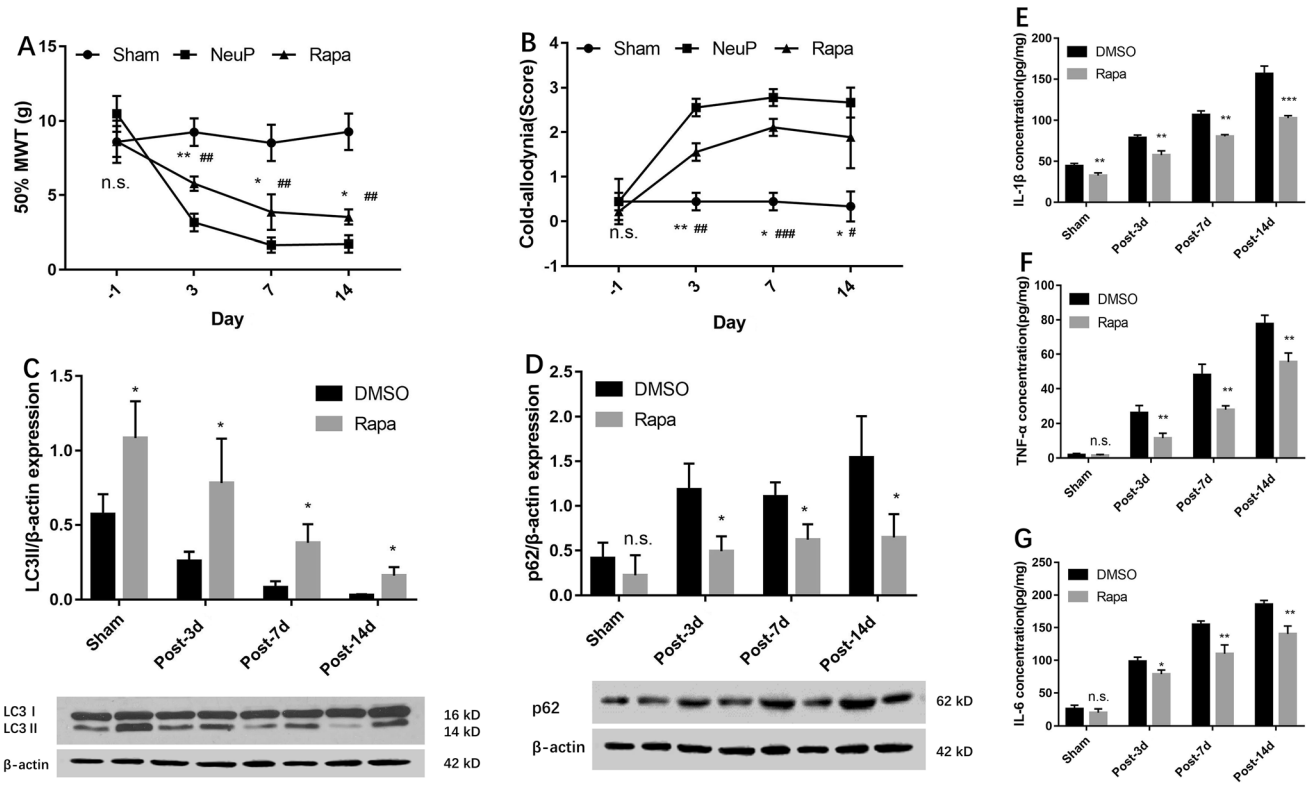

Fig. 5 Upregulation of autophagy suppresses neuroinflammation and attenuates neuropathic pain. **A**, **B** The 50%MWT (**A**) and CWS (**B**) in the sham and neuropathic pain groups after rapamycin treatment from day 3 to day 14 post-surgery (mean ± SD; $n = 8$; n.s., no significant difference among Sham, NeuP and GSK126 groups; $^{*}P < 0.05$, $^{**}P < 0.01$ *vs* NeuP group; $^{\#}P < 0.05$, $^{\#\#}P < 0.01$, $^{\#\#\#}P < 0.001$ *vs* Sham group). **C**, **D** Relative expression of LC3II (**C**) and p62 protein (**D**) in the ACC of the Sham and NeuP groups after rapamycin treatment compared with DMSO treatment from day 3 to day 14 post-surgery. **E**–**G** ELISA analysis of the IL-1β (**E**), TNF-α (**F**), and IL-6 (**G**) expression levels in the ACC of the Sham and NeuP groups after rapamycin treatment from day 3 to day 14 post-surgery. For **C**–**G**: mean ± SD; $n = 8$; n.s., no significant difference; $^{*}P < 0.05$, $^{**}P < 0.01$, $^{***}P < 0.001$, *vs* DMSO group.

number of studies have shown that neuropathic pain might be caused by comprehensive alterations in neurons and glial cells, particularly microglia [23]. Microglia constitute the major population of glial cells in the CNS, supporting the hypothesis that they play a leading role in regulating neuroinflammation [24]. Signaling molecules released following peripheral nerve injury may activate microglia in the CNS, causing them to release pro-inflammatory cytokines and chemokines such as IL-1β, TNF-α, IL-6, and brain-derived neurotrophic factor, which play primary key roles in initiating and maintaining neuropathic pain [25, 26]. Recent studies regarding the role of microglia in neuropathic pain have mainly focused on the dorsal horn of the spinal cord [7]; however, the underlying mechanisms by which microglia modulate neuropathic pain in the ACC remain poorly understood.

Evidence has shown that epigenetic alterations may initiate and maintain neuropathic pain [27, 28], while the EZH2-mediated histone modification of gene expression has been shown to correlate with human cancers, including prostate cancer, colorectal cancer, and lymphoma [29–32]. Moreover, abnormal EZH2 has been associated with the inflammatory response and neurodegeneration. For instance, Zhang *et al.* [33] reported that EZH2 induces pro-inflammatory gene expression by mediating toll-like receptors, and EZH2 depletion attenuates autoimmune inflammation in colitis and autoimmune encephalomyelitis. In addition, EZH2 expression is upregulated in rats with chronic sciatic nerve injury-induced neuropathic pain, and its overexpression reverses the decreased pro-inflammatory cytokines expression [11].

In this study, we investigated whether abnormal EZH2 expression affects the secretion of pro-inflammatory cytokines and the pathophysiology of neuropathic pain in rats with BPA-induced neuropathic pain. We showed that EZH2 expression was strongly upregulated in NeuP rats, while inhibiting EZH2 decreased the IL-1β, TNF-α, and IL-6 secretion. More importantly, inhibiting EZH2 decreased the mechanical and cold allodynia. Therefore, our results suggest that EZH2 plays a role in the molecular mechanisms of neuropathic pain.

Consequently, we also investigated the molecular mechanisms by which EZH2 regulates neuropathic pain. Autophagy is a key process that regulates immunity and

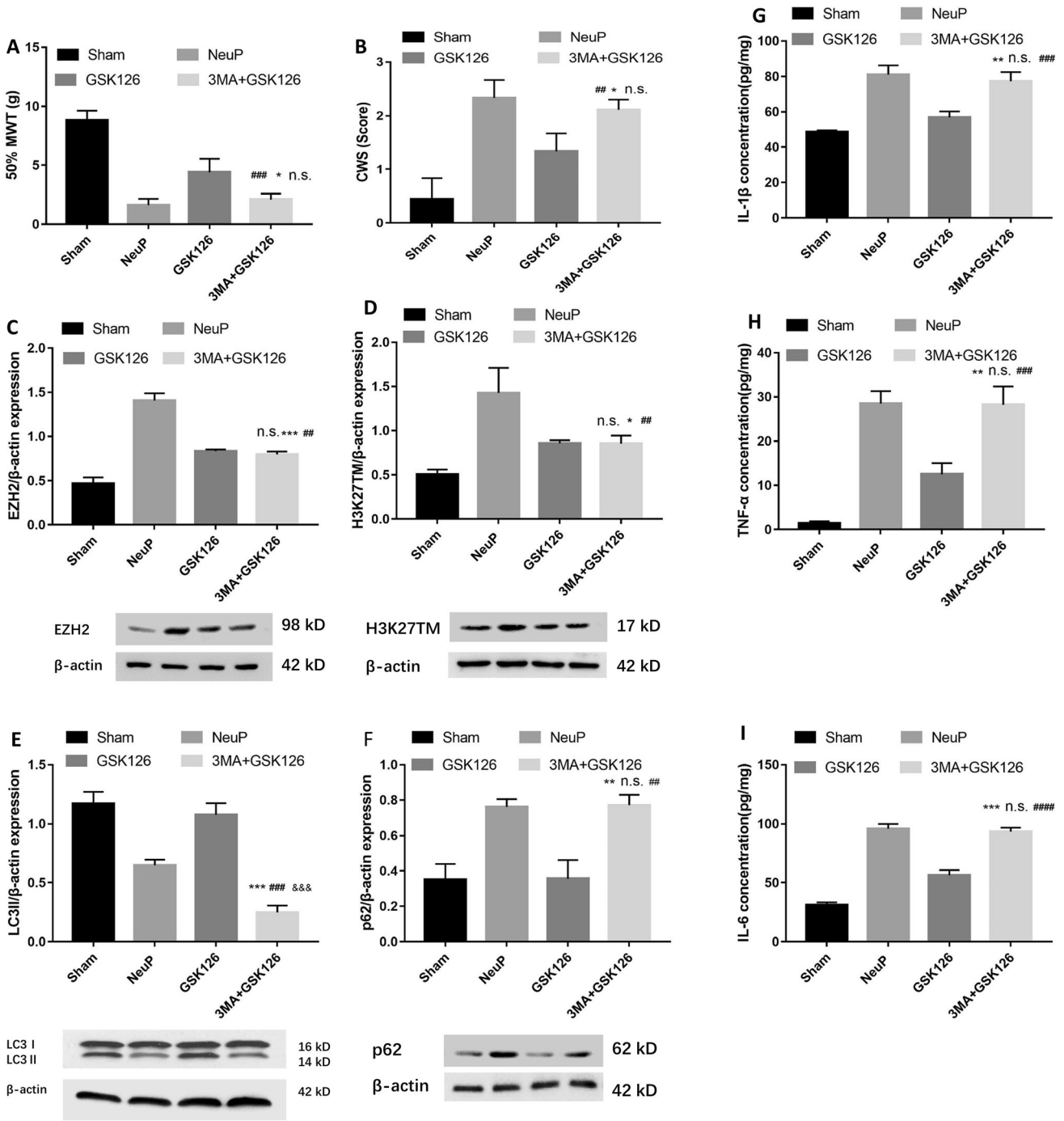

Fig. 6 Inhibition of autophagy by 3-MA impairs EZH2 inhibitor-induced pain relief and neuroinflammation remission. **A**, **B** Mechanical allodynia (**A**) and cold allodynia (**B**) in sham-operated and neuropathic pain groups after 3-MA combined with GSK126 treatment from day 1 to day 3 post-surgery (mean ± SD; $n = 8$; n.s., no significant difference *vs* NeuP group; $^{*}P < 0.05$ *vs* GSK126 group; $^{\#\#}P < 0.01$, $^{\#\#\#}P < 0.001$ *vs* Sham group). **C**–**F** Relative expression of EZH2 (**C**) and H3K27TM (**D**) (mean ± SD; $n = 8$; n.s., no significant difference *vs* GSK126 group; $^{*}P < 0.05$, $^{***}P < 0.001$ *vs* NeuP group; $^{\#\#}P < 0.01$ *vs* Sham group), LC3II (**E**) (mean ± SD; $n = 8$; $^{***}P < 0.001$ *vs* NeuP group; $^{\#\#\#}P < 0.001$ *vs* GSK126 group; $^{\&\&\&}P < 0.001$ *vs* Sham group), and p62 protein (**F**) (mean ± SD; $n = 8$; $^{**}P < 0.01$ *vs* GSK126 group; n.s., no significant difference *vs* NeuP group; $^{\#\#}P < 0.01$ *vs* Sham group) in the ACC of rats after 3-MA combined with GSK126 treatment from day 1 to day 3 post-surgery. **G**–**I** ELISA analysis of IL-1β (**G**), TNF-α (**H**), and IL-6 (**I**) expression levels in the ACC of the Sham and NeuP groups after 3-MA combined with GSK126 treatment from day 1 to day 3 post-surgery (mean ± SD; $n = 8$; n.s., no significant difference *vs* NeuP group; $^{**}P < 0.01$, $^{***}P < 0.001$ *vs* GSK126 group; $^{\#\#\#}P < 0.001$, $^{\#\#\#\#}P < 0.0001$ *vs* Sham group).

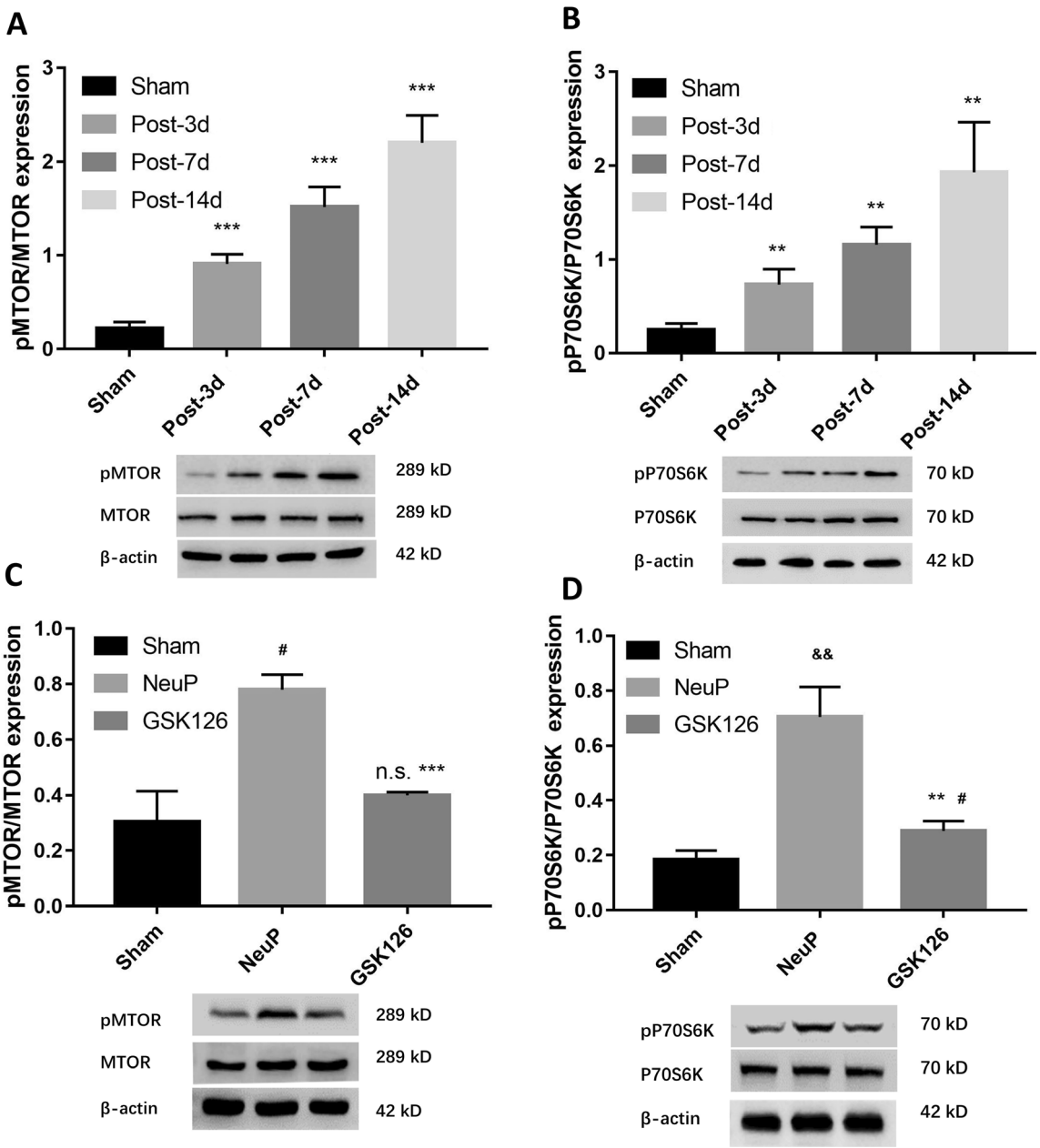

Fig. 7 EZH2 regulates autophagy *via* an MTOR-dependent signaling pathway. **A–D** Relative expression of pMTOR (**A**) and pP70S6K (**B**) (mean ± SD; $n = 8$; $^{**}P < 0.01$, $^{***}P < 0.001$ *vs* Sham group), pMTOR (**C**) (mean ± SD; $n = 8$; $^{***}P < 0.001$ *vs* NeuP group; n.s., no significant difference *vs* Sham group; $^{\#}P < 0.05$ *vs* Sham group), and pP70S6K (**D**) (mean ± SD; $n = 8$; $^{**}P < 0.01$ *vs* NeuP group; $^{\#}P < 0.05$ *vs* Sham group; $^{\&\&}P < 0.01$ *vs* Sham group) in the ACC of rats after GSK126 treatment from day 1 to day 3 post-surgery.

inflammation; several studies have demonstrated a relationship between EZH2 and autophagy in the etiology of diseases such as colorectal cancer and laryngeal squamous cell carcinoma. However, their regulatory mechanisms have not yet been elucidated [34, 35]. It has also been suggested that EZH2 may affect autophagy *via* microRNA, STAT, or fuse-binding protein 1-c-Myc in osteoarthritis, breast cancer, endometrial carcinoma, cholangiocarcinoma, and osteosarcoma, while the signaling pathway by which EZH2 regulates autophagy has not yet been confirmed [36–40]. In this study, we found that pharmacologically inhibiting EZH2 promoted the suppression of autophagy induced by BPA, while inhibiting autophagy activation impaired the GSK126-induced reduction of neuroinflammation and neuropathic pain. Therefore, these findings indicate that autophagy activity acts downstream of EZH2 and is involved in neuropathic pain.

To improve our understanding of the effect of autophagy on neuropathic pain, we used Rapa to reveal the pathophysiology of BPA-induced neuropathic pain. We found that increasing autophagy with Rapa suppressed neuropathic pain and the release of pro-inflammatory cytokines while reducing MTOR phosphorylation. These data suggested that autophagy negatively regulates neuroinflammation via the MTOR signaling pathway, and this could be the direct cause of neuropathic pain. Although our results revealed that EZH2 regulated autophagy *via* the MTOR pathway, we were unable to determine how EZH2 phosphorylates MTOR in nerve injury-induced neuropathic pain. However, it has been shown that EZH2 regulates TSC2 (tuberous sclerosis complex 2) expression by interacting with MTA2 (metastasis-associated 1 family member 2), and subsequently phosphorylates MTOR [21]. To our knowledge, this is the first study to identify a specific autophagy regulatory molecule that is regulated by EZH2. Recently, another study found that inhibiting EZH2 reduces phosphorylated AKT expression and thus represses pMTOR production in pancreatic cancer [41], suggesting that EZH2 regulates MTOR phosphorylation *via* the AKT signaling pathway. These studies provide possible directions for future research to elucidate how EZH2 regulates autophagy *via* the MTOR pathway.

In conclusion, we found that targeting the EZH2/autophagy signaling pathway is a promising option for regulating neuroinflammation and managing neuropathic pain. Thus, our findings suggest a novel approach for treating BPA-induced neuropathic pain.

Acknowledgements We thank Yudong Gu, Ji-feng Li, Qi-Liang Mao-Ying, and Yong Bao for kindly providing assistance with experimental design and technology support. This work was supported by the National Natural Science Foundation of China (81572127).

Conflict of interest The authors claim that there are no conflicts of interest.

References

1. Jensen TS, Baron R, Haanpää M, Kalso E, Loeser JD, Rice AS, *et al.* A new definition of neuropathic pain. Pain 2011, 152: 2204–2205.
2. Teixeira MJ, da Paz MG, Bina MT, Santos SN, Raicher I, Galhardoni R, *et al.* Neuropathic pain after brachial plexus avulsion-central and peripheral mechanisms. BMC Neurol 2015, 15: 73.
3. Iannetti GD, Mouraux A. From the neuromatrix to the pain matrix (and back). Exp Brain Res 2010, 205: 1–12.
4. Chen T, Taniguchi W, Chen QY, Tozaki-Saitoh H, Song Q, Liu RH, *et al.* Top–down descending facilitation of spinal sensory excitatory transmission from the anterior cingulate cortex. Nat Commun 2018, 9: 1886–1902.
5. Yang Z, Tan Q, Cheng D, Zhang L, Zhang J, Gu EW, *et al.* The changes of intrinsic excitability of pyramidal neurons in anterior cingulate cortex in neuropathic pain. Front Cell Neurosci 2018, 12: 436.
6. Shi G, Shi J, Liu K, Liu N, Wang Y, Fu Z, *et al.* Increased miR-195 aggravates neuropathic pain by inhibiting autophagy following peripheral nerve injury. Glia 2013, 61: 504–512.
7. Tsuda M. Microglia of pain and itch by spinal glia. Neurosci Bull 2018, 34: 178–185.
8. Wang B, Fan B, Dai Q, Xu X, Jiang P, Zhu L, *et al.* Fascin-1 contributes to neuropathic pain by promoting inflammation in rat spinal cord. Neurochem Res 2018, 43: 287–296.
9. Yadav R, Weng HR. EZH2 regulates spinal neuroinflammation in rats with neuropathic pain. Neuroscience 2017, 349: 106–117.
10. Arifuzzaman S, Das A, Kim SH, Yoon T, Lee YS, Jung KH, *et al.* Selective inhibition of EZH2 by a small molecule inhibitor regulates microglial gene expression essential for inflammation. Biochem Pharmacol 2017, 137: 61–80.
11. Zhang Y, Liu HL, An LJ, Li L, Wei M, Ge DJ, *et al.* miR-124-3p attenuates neuropathic pain induced by chronic sciatic nerve injury in rats via targeting EZH2. J Cell Biochem 2019, 120: 5747–5755.
12. Menzies FM, Fleming A, Caricasole A, Bento CF, Andrews SP, Ashkenazi A, *et al.* Autophagy and neurodegeneration: pathogenic mechanisms and therapeutic opportunities. Neuron 2017, 93: 1015–1034.
13. Yang Z, Klionsky DJ. Eaten alive: a history of macroautophagy. Nat Cell Biol 2010, 12: 814–822.
14. Zhang E, Yi MH, Ko Y, Kim HW, Seo JH, Lee YH, *et al.* Expression of LC3 and Beclin 1 in the spinal dorsal horn following spinal nerve ligation-induced neuropathic pain. Brain Res 2013, 1519: 31–39.
15. Guo JS, Jing PB, Wang JA, Zhang R, Jiang BC, Gao YJ, *et al.* Increased autophagic activity in dorsal root ganglion attenuates neuropathic pain following peripheral nerve injury. Neurosci Lett 2015, 599: 158–163.
16. Wang L, Yuzhou L, Yingjie Z, Jie L, Xin Z. A new rat model of neuropathic pain: complete brachial plexus avulsion. Neurosci Lett 2015, 589: 52–56.
17. Willemen HL, Eijkelkamp N, Wang H, Dantzer R, Dorn GW 2nd, Kelley KW, *et al.* Microglial/macrophage GRK2 determines duration of peripheral IL-1beta-induced hyperalgesia: contribution of spinal cord CX3CR1, p38 and IL-1 signaling. Pain 2010, 150: 550–560.
18. Rubens RF, Adair RS, Jayme AB, João BC. Avulsion injury of the rat brachial plexus triggers hyperalgesia and allodynia in the hindpaws. Brain Res 2003, 982: 186–194.
19. Dixon WJ. Efficient analysis of experimental observations. Annu Rev Pharmacol Toxicol 1980, 20: 441–462.
20. Choi Y, Yoon YW, Na HS, Kim SH, Chung JM. Behavioral signs of ongoing pain and cold allodynia in a rat model of neuropathic pain. Pain 1994, 59: 369–376.
21. Wei FZ, Cao Z, Wang X, Wang H, Cai MY, Li T, *et al.* Epigenetic regulation of autophagy by the methyltransferase EZH2 through an MTOR-dependent pathway. Autophagy 2015, 11: 2309–2322.
22. Fujita N, Itoh T, Omori H, Fukuda M, Noda T, Yoshimori T. The Atg16L complex specifies the site of LC3 lipidation for membrane biogenesis in autophagy. Mol Biol Cell 2008, 19: 2092–2100.
23. Ji RR, Chamessian A, Zhang YQ. Pain regulation by non-neuronal cells and inflammation. Science 2016, 354: 572–577.
24. Brifault C, Kwon H, Campana WM, Gonias SL. LRP1 deficiency in microglia blocks neuro-inflammation in the spinal dorsal horn and neuropathic pain processing. Glia 2019, 67: 1210–01224.

25. Kiguchi N, Kobayashi D, Saika F, Matsuzaki S, Kishika S. Pharmacological Regulation of Neuropathic Pain Driven by Inflammatory Macrophages. Int J Mol Sci 2017, 18: 2296–2311.
26. Gong X, Chen Y, Chang J, Huang Y, Cai M, Zhang M. Environmental enrichment reduces adolescent anxiety- and depression-like behaviors of rats subjected to infant nerve injury. J Neuroinflammation 2018, 15: 262.
27. Penas C, Navarro X. Epigenetic modifications associated to neuroinflammation and neuropathic pain after neural trauma. Front Cell Neurosci 2018, 12: 158.
28. Feng XL, Deng HB, Wang ZG, Wu Y, Ke JJ, Feng XB. Suberoylanilide hydroxamic acid triggers autophagy by influencing the mTOR pathway in the spinal dorsal horn in a rat neuropathic pain model. Neurochem Res 2019, 44: 450–0464.
29. Wang D, Ding L, Wang L, Zhao Y, Sun Z, Karnes RJ, *et al.* LncRNA MALAT1 enhances oncogenic activities of EZH2 in castration-resistant prostate cancer. Oncotarget 2015, 6: 41045–041055.
30. Wang X, Sehgal L, Jain N, Khashab T, Mathur R, Samaniego F. LncRNA MALAT1 promotes development of mantle cell lymphoma by associating with EZH2. J Transl Med 2016, 14: 346.
31. Li P, Zhang X, Wang H, Wang L, Liu T, Du L, *et al.* MALAT1 is associated with poor response to oxaliplatin-based chemotherapy in colorectal cancer patients and promotes chemoresistance through EZH2. Mol Cancer Ther 2017, 16: 739–0751.
32. Yamagishi M, Uchimaru K. Targeting EZH2 in cancer therapy. Curr Opin Oncol 2017, 29: 375–0381.
33. Zhang X, Wang Y, Yuan J, Li N, Pei S, Xu J, *et al.* Macrophage/microglial Ezh2 facilitates autoimmune inflammation through inhibition of Socs3. J Exp Med 2018, 215: 1365–01382.
34. Yao Y, Hu H, Yang Y, Zhou G, Shang Z, Yang X, *et al.* Downregulation of enhancer of zeste homolog 2 (EZH2) is essential for the induction of autophagy and apoptosis in colorectal cancer cells. Genes (Basel) 2016, 7: E83.
35. Chen L, Jia J, Zang Y, Li J, Wang B. MicroRNA-101 regulates autophagy, proliferation and apoptosis via targeting EZH2 in laryngeal squamous cell carcinoma. Neoplasma 2019, 66: 507–0515.
36. Lian WS, Ko JY, Wu RW, Sun YC, Chen YS, Wu SL, *et al.* MicroRNA-128a represses chondrocyte autophagy and exacerbates knee osteoarthritis by disrupting Atg12. Cell Death Dis 2018, 9: 919.
37. Liu F, Sang M, Meng L, Gu L, Liu S, Li J, *et al.* miR-92b promotes autophagy and suppresses viability and invasion in breast cancer by targeting EZH2. Int J Oncol 2018, 53: 1505–1515.
38. Wang C, Liu B. miR-101-3p induces autophagy in endometrial carcinoma cells by targeting EZH2. Arch Gynecol Obstet 2019, 297: 1539–1548.
39. Ma J, Weng L, Wang Z, Jia Y, Liu B, Wu S, *et al.* MiR-124 induces autophagy-related cell death in cholangiocarcinoma cells through direct targeting of the EZH2-STAT3 signaling axis. Exp Cell Res 2018, 366: 103–113.
40. Xiong X, Zhang J, Liang W, Cao W, Qin S, Dai L, *et al.* Fuse-binding protein 1 is a target of the EZH2 inhibitor GSK343, in osteosarcoma cells. Int J Oncol 2016, 49: 623–628.
41. Xu H, Zhang L, Qian X, Zhou X, Yan Y, Zhou J, *et al.* GSK343 induces autophagy and downregulates the AKT/mTOR signaling pathway in pancreatic cancer cells. Exp Ther Med 2019, 18: 2608–2616.